The Spectral Energy Distribution of the Seyfert galaxy Ton S180[1]

T. J. Turner[1,2], P. Romano[3], S. B. Kraemer[4,5], I. M. George[1,2], T. Yaqoob[1,6], D. M. Crenshaw[7], J. Storm[8], D. Alloin[9], D. Lazzaro[10], L. Da Silva[10], J. D. Pritchard[9], G. Kriss[6,11], W. Zheng[6], S. Mathur[3], J. Wang[6], P. Dobbie[12], N. R. Collins[4,5,13]

ABSTRACT

[1]Joint Center for Astrophysics, Physics Dept., University of Maryland Baltimore County, 1000 Hilltop Circle, Baltimore, MD 21250

[2]Laboratory for High Energy Astrophysics, Code 662, NASA/GSFC, Greenbelt, MD 20771

[3]Department of Astronomy, The Ohio State University, 140 West Avenue, Columbus, OH 43210

[4]Laboratory for Astronomy and Solar Phyiscs, Code 661, NASA/GSFC, Greenbelt, MD 20771

[5]Institute for Astrophysics and Computational Sciences, The Catholic University of America Washington, DC 20064

[6]Center for Astrophysical Sciences, Department of Physics and Astronomy, The Johns Hopkins University, Baltimore, MD 21218

[7]Department of Physics and Astronomy, Georgia State University, Atlanta, GA 30303

[8]AIP, An der Sternwarte 16, D-14482 Potsdam, Germany

[9]European Southern Observatory, Casilla 19001, Santiago, Chile

[10]Observatorio Nacional, Departamento de Astronomia, Rua Gen. Jose Cristino, 77, 20921-400, Rio de Janeiro, Brazil Observatorio Nacional, Rio de Janeiro, Brazil

[11]Space Telescope Science Institute, 3700 San Martin Drive, Baltimore, MD 21218

[12]Astronomy Group, Leicester University, Leicester LE1 7RH, UK

[13]Science Systems and Applications, Inc., 5900 Princess Garden Parkway Suite 300, Lanham, MD 20706

We present spectral results from a multi-satellite, broad-band campaign on the Narrow-line Seyfert 1 galaxy Ton S180 performed at the end of 1999. We discuss the spectral-energy distribution of the source, combining simultaneous *Chandra*, *ASCA* and *EUVE* data with contemporaneous *FUSE*, *HST*, and ground-based optical and infra-red data. The resulting SED shows that most of the energy is emitted in the 10 – 100 eV regime, which must be dominated by the primary energy source. No spectral turnover is evident in the UV regime. This, the strong soft X-ray emission, and the overall shape of the SED indicate that emission from the accretion disk peaks between 15 and 100 eV. High resolution *FUSE* spectra showing UV absorption due to OVI and the lack of detectable X-ray absorption in the *Chandra* spectrum demonstrate the presence of a low column density of highly ionized gas along our line-of-sight.

The highly-ionized state of the circumnuclear gas is most likely linked to the high luminosity and steep spectrum of the active nucleus. Given the strong ionizing flux in Ton S180, it is possible that the clouds within a few tens of light days of the central source are too highly ionized to produce much line emission. Thus the narrow width of the emission lines in Ton S180 is due to the emission arising from large radii.

Subject headings: galaxies: active – galaxies: individual (Ton S180) – galaxies: nuclei – galaxies: Seyfert

1. Introduction

A longstanding suggestion has been that there is a so-called "big-blue-bump" (BBB) of continuum emission, peaking in the unseen X-ray to UV (XUV) regime, perhaps originating in the accretion disk. There are indications of the low energy tail of this component in the UV spectra of Seyfert 1 galaxies (**?**)]Shields78,MalkanSa82. The peak energy of the disk emission is predicted to be dependent on the accretion rate (**?**)]MFR93b. Thus the spectral-energy-distribution (SED) of an AGN provides crucial information about accretion rates and conditions close to the disk. However, determination of the XUV continuum in AGN has been extremely difficult because of the severe attenuation of photons of these energies by even small amounts of Galactic material along the line-of-sight. Some indication of the strength of the unseen continuum has been inferred from the strengths of emission lines such

[1]Based (in part) on observations made with the Danish 1.5m telescope at ESO, La Silla, Chile

as He IIλ1640 (**?**, e.g.)]MathewsF87. Zheng et al. (1997) have suggested the form of the unseen XUV spectrum is $f_v \propto v^{-\alpha}$ with $\alpha = 2$ between the Lyman limit (at 912 Å) and $\sim 0.5\,$keV. Laor et al. (1997) combine this with a mean soft X-ray spectrum, based upon *ROSAT* observations of quasars, to dispute the existence of a large XUV bump. Telfer et al. (2002) extend the work of Zheng et al. (1997) by including more data in the extreme UV band; those authors find the data to be adequately represented by a simple power-law with $\alpha = 1.76$ between 500 and 1200 Å. **?**)][]KoristaFB97 have discussed the problem that extrapolating the known soft X-ray spectrum of AGN, there appear to be too few 54.4 eV photons to account for the strength of the observed He II lines. They consider the possibility that the broad-line clouds see a harder continuum than the observer does, or that the XUV spectrum has a double-peaked shape.

Narrow-line Seyfert 1 galaxies (NLSy1s) were first classified on the basis of their unusual optical properties, most notably, lying at the lower end of the distribution of line widths, for permitted optical lines. Specifically, widths of Hβ FWHM $< 2000\,$km s^{-1} have been taken as the defining quality of NLSy1s, although it is widely acknowledged that this value is arbitrary and there is a continuous range of broad-band properties across the Seyfert population. Nevertheless, the distinction is useful, as an object's place in the line-width distribution of the Seyfert population is an indicator of other properties, especially the X-ray properties. NLSy1s appear to have systematically different, or very extreme X-ray attributes compared to the rest of the Seyfert population, which we will henceforth refer to as broad-line-Seyfert 1s (BLSy1s). For example, examination of X-ray properties across the Seyfert population reveals that FWHM Hβ is strongly anti-correlated with the excess variance σ^2_{RMS} (Turner et al. 1999a; where $\sigma^2_{\rm RMS} = \frac{1}{N\mu^2}\sum_{i=1}^{N}[(X_{\rm i}-\mu)^2 - \sigma^2_{\rm i}]$ for a light curve with N points of counts $X_{\rm i}$ and unweighted mean μ) and anti-correlated with X-ray index, in the sense that NLSy1s are most variable and have steeper spectra (Boller, Brandt, & Fink 1996; Brandt, Mathur, & Elvis 1997). These correlations suggest a fundamental difference between BLSy1s and NLSy1s, the latter being thought to represent the low mass and/or high accretion-rate systems (**?**, e.g.)]PDO95.

For black holes operating near $L_{\rm Edd}$, the accretion disk surface is predicted to be highly ionized, thus the disk spectrum is expected to peak at higher energies in NLSy1s than in BLSy1s. In the soft X-ray regime the NLSy1s Ton S180 and Arakelian 564 (Akn 564) show a hump of emission close to 1 keV (**?**, e.g.)]TGN98,Vaughan99a,Turnerea01,Akn564I, which could be the signature of a hot disk. Fiore et al. (1998) also suggested an ionized disk as the origin of a soft X-ray component in PG 1244+026. Interestingly, at least nine AGN are known to possess a soft hump with characteristic shape as described for Ton S180. These AGN are all NLSy1s: PG 1244+026 (Fiore et al. 1998; George et al. 2000); IRAS 13224-3809 (Vaughan et al. 1999b); Akn 564 (Brandt et al. 1994; Turner, George, & Netzer 1999); NGC 4051

(Collinge et al. 2001); PG 1404+226, PG 1440+356 (Mkn 478), and PG 1211+143 (George et al. 2000); Ton S180 (Turner, George, & Nandra 1998; Turner et al. 2001a); 1H 0707-495 (Boller et al. 2001). Further evidence for an ionized disk comes from the observation of Fe Kα emission from ionized gas in numerous NLSy1s (Comastri et al. 1998; Turner, George, & Nandra 1998; Turner, George, & Netzer 1999; Vaughan et al. 1999b; Comastri et al. 2001; Ballantyne, Iwasawa, & Fabian 2001).

Thus examination of the SED of a NLSy1, and comparison with that obtained for BLSy1s should offer insight into the relative accretion rates across the Seyfert population. To this end, we undertook a multi-wavelength campaign to obtain a broad-band spectral-energy-distribution of Ton S180.

2. Ton S180

We selected Ton S180 for study as it is bright in the soft X-ray regime and has low line-of-sight and intrinsic extinction, allowing a view of the bare continuum form. Ton S180 (PHL 912, z=0.06198; Wisotzki et al. 1995) has a low Galactic column density along the line-of-sight, $N_{\rm H} = 1.55^{+0.27}_{-0.13} \times 10^{20}$ cm^{-2} (Dickey & Lockman 1990). The uncertainty on the column density represents the maximum scatter of values of column density within a 1 degree cone centered on Ton S180. The observed flux (i.e. no correction for extinction) is $F_{0.5-2\,\rm keV} \sim 1.1 \times 10^{-11}$ ergs s^{-1} cm^{-2} (Turner, George, & Nandra 1998). The source is at the extreme end of the Seyfert range of line widths with FWHM Hα and H$\beta \sim 900$ km s^{-1}, making it a good choice for isolating the fundamental parameter which determines the classification of a Seyfert galaxy.

BeppoSAX (Comastri et al. 1998) and *ASCA* (Turner, George, & Nandra 1998) data from Ton S180 indicated a steep spectrum in the 2–10 keV band, with $\alpha = 1.5$; both datasets also showed an Fe Kα emission line peaked at a rest-energy ~ 7 keV, indicating that the circumnuclear material is strongly ionized. *ASCA* data confirm the complexity of the soft X-ray spectrum first noted in *ROSAT* PSPC data (Fink et al. 1997). A *Chandra* Low Energy Transmission Grating (LETG) observation has recently revealed the soft hump component to be a smooth continuum or extremely broadened reprocessed component (Turner et al. 2001a).

In this paper we use energy index α for quantification of spectral indices, defined such that the flux density $F(E) \propto E^{-\alpha}$ at energy E. A log of the observations performed in support of the campaign is presented in Table 1. All the data were reduced using standard techniques as outlined below.

3. ASCA

3.1. Data Reduction

The *ASCA* satellite carries four focal-plane detectors, two CCDs (the Solid-state Imaging Spectrometers or SISs, covering 0.4-10.0 keV) and two Gas Imaging Spectrometers (GISs, covering 0.7-10.0 keV), all are operated simultaneously. *ASCA* observed Ton S180 for a baseline of 12 days, $\sim$ 1Ms, 1999 December 3 – 15. Those data were reduced using the methods and screening criteria of the *Tartarus* (Turner et al. 1999b) database. As reported by Romano et al. (2002) these screening criteria resulted in an effective exposure of 405 ks in the GISs, 338 ks and 368 ks in SIS0 and SIS1, respectively. The mean SIS0 count rate was 0.586 ± 0.001 ct s^{-1}. The data were reduced using the calibration file `sisph2pi_290301.fits` and the degradation of the low-energy response of the SISs was compensated for by the time-dependent absorption term detailed by Yaqoob et al. (2000)[15]. Romano et al. (2002) utilized corrections of $N_H = 6.9\times10^{20}$cm^{-2} and $N_H = 1.0\times10^{21}$cm^{-2} for SIS0 and SIS1, respectively. The results presented here are primarily based on the analysis of the time-averaged spectra obtained during the simultaneous *ASCA*–*Chandra* observations. This means that while all of the *Chandra* data were used, only a subset of the *ASCA* data were utilized. Figure 1 shows the periods covered by the *FUSE* and *Chandra* observations, with respect to the entire 12-day observation by *ASCA*, allowing us to see where these new datasets lie compared to the recent flux history of the source. Figure 2, shows in detail the *Chandra* light curve with part of the overlapping *ASCA* dataset. In this paper, we use only the mean *ASCA* spectrum from the period simultaneous with the *Chandra* observation, i.e. within JD 2451526.576 – 2451527.498.

3.2. ASCA Results

As is evident from Figure 2, Ton S180 exhibited significant changes in flux. Romano et al. (2002) present a detailed analysis of spectral variability over the full 12-day observation. Romano et al. (2002) find the continuum fit to the mean spectrum to yield $\alpha = 1.44\pm0.02$. A strong excess of emission is observed below 2 keV, and this soft component varies in strength down to the minimum timescale determinable via spectral analysis, $\sim$ 1 day. The variations in hump strength are correlated with the photon index and the 2-10 keV flux, consistent with disk-corona models (Romano et al. 2002). The softness ratio shows rapid variability on timescales < 1000 s, indicating either a breakdown of the correlation between soft hump

[15]see http://heasarc.gsfc.nasa.gov/docs/asca/calibration/nhparam.html

and power-law fluxes on such short timescales, or rapid variations in the photon index. Romano et al. (2002) also find a broad Fe Kα line with narrow peak at a rest-energy 6.8 keV, indicating an origin in ionized material.

Analysis of the spectrum acquired simultaneously with *Chandra* data reveals $\alpha = 1.44 \pm 0.07$ (in agreement with the mean for the full dataset). The soft component shows an equivalent width EW $= 63^{+71}_{-50}$ eV when parameterized using a Gaussian model. As Romano et al. (2002) found no evidence for variability in the flux or equivalent width of the Fe Kα line we do not fit for the Fe Kα parameters here (and exclude the 5.0-7.5 keV data when fitting for continuum slopes).

4. Chandra

4.1. ACIS/LETG Data Reduction

The *Chandra* data were reprocessed using calibration files from `CALBD v2.6`. the data were then screened to remove bad pixels, columns and events with detector 'grades' *not* equal to 0, 2, 3, 4, or 6. Periods of high background were also excluded. Such screening resulted in an on-source exposure of ∼75 ks. The 1^{st}-order spectra were extracted from the screened event file and appropriate ancillary response files constructed using `CIAO v2.1`. Previous analysis of these data (Turner et al. 2001a) was limited to use of data above ~ 0.4 keV, due to unacceptable uncertainty in the ACIS/LETG calibration around the C-edge. However, the quantum efficiency (QE) file `acisD1997-04-17qeN0004.fits`, released 2001-06-07, was utilized in the analysis presented here, this improves the fit to ACIS/LETG observations of calibration sources, in the C-edge regime. Utilization of the new quantum efficiency file allows examination of data down to 0.2 keV, the lowest energy available from LETG data with ACIS in the focal plane. The entire *Chandra* baseline is utilized in this analysis, as the *ASCA* observation overlaps the *Chandra* observation completely (Figure 2).

4.2. LETG Results

In Figure 2 we show the light curve obtained from the $\pm 1^{st}$-order *Chandra*/LETG data. The portion of the *ASCA* SIS light curve (from Figure 2) is overlaid for direct comparison. As might be expected, there is good agreement between the light curves from the two instruments.

Turner et al. (2001a) present the first order LETG spectra of Ton S180, finding no strong spectral features and concluding that the excess soft X-ray emission discovered using *ASCA* (Turner, George, & Nandra 1998) must be primarily due to a previously-unknown *continuum* component or very broadened reprocessed component. Turner et al. (2001a) note the lack of strong absorption features in the X-ray spectrum of Ton S180, in contrast to results from many Seyfert 1 galaxies (e.g. the BLSy1s NGC 5548, Kaastra et al. 2000, and NGC 3783 Kaspi et al. 2000, and the NLSy1 NGC 4051, Collinge et al. 2001). Analysis using the new QE file reveals an improvement to the agreement between *ASCA* and LETG data in the 1-2 keV regime (c.f. results presented by Turner et al. 2001a). We also re-examined the shape of the soft excess. The extrapolation of the hard-band power-law to soft X-ray energies reconfirms the presence of excess soft emission as expected, with a sharp turnover of the data below $\sim 0.3\,\mathrm{keV}$ ($\sim 7 \times 10^{16}\,\mathrm{Hz}$). Figure 3 shows the form of the soft component. The turnover is sharper than that expected due to absorption by edges in neutral or ionized gas. In any case, if there were such a deep absorption edge in the X-ray regime, strong spectral features would be expected in other parts of the spectrum, which are not observed. The soft hump in the data was modeled using the XSPEC DISKBB model (Mitsuda et al. 1984; Makishima et al. 1986). However, although DISKBB has some intrinsic spectral curvature, this was not able to account for the shape of the LETG data. A fit to data above 0.3 keV yielded a best-fit temperature of ~ 98 eV at the inner edge of the disk. Possible explanations for the apparent shape of the soft excess include continuing problems with the softest energy calibration, and the more intriguing possibility of a peak due to the presence of a blend of broadened emission lines as suggested previously for some Seyfert galaxies (Branduardi-Raymont et al. 2001; Turner et al. 2001a). Comastri et al. (1998) present a *BeppoSAX* spectrum of Ton S180 down to ~ 0.1 keV, with no evidence for a spectral drop below 0.3 keV, supporting the possibility that this is due to residual calibration problems in the LETG. Thus we do not perform detailed fitting to this feature.

5. EUVE

Archival *EUVE* data are available covering a period which overlaps the *Chandra* observation. We processed these data using standard techniques. Source counts were summed in a circular aperture of 25 pixels in radius and the background calculated from a surrounding annulus of 30 pixels in width. The deadtime-Primbsching correction was used to correct the count rate for the loss of events due to the deadtime of the detector electronics and "primbsching" caused by the rather limited width of the telemetry buffer. A standard technique calls for data with a deadtime-Primbsching correction (DPC) factor > 1.25 to be discarded, as the systematic errors present in the estimates of this correction factor increase with its

magnitude. However, during the course of reducing these data it was noted that the DS DPC factor frequently lay above 1.5, significantly greater than the more typically observed values of 1.0-1.3. This was likely due to increased geocoronal emission possibly associated with the approaching solar maximum at that epoch and/or the decreasing orbital altitude of the *EUVE* satellite. These conditions forced us to select data between the more liberal limits of 1.0 <DPC< 2.0 in order to have adequate counts for construction of a spectrum for the time period simultaneous with the *ASCA* and LETG overlap observation. The effective on-source exposure was 21 ks within the start and stop times determined from the LETG observation. The background-subtracted count rate for the full-band was $7.1 \pm 3.7 \times 10^{-3}$cm s^{-1}.

6. FUSE

6.1. Data Reduction

We used *FUSE* to obtain the 905–1187 Å far-UV spectrum of Ton S180 on 1999 December 12, 05:50:32–19:41:14 UT. The total observing time was 15.2 ks. For a full description of *FUSE* and its initial in-flight performance, see Moos et al. (2000) and Sahnow et al. (2000). Briefly, four separate primary mirrors in *FUSE* collect light to feed four prime-focus, Rowland-circle spectrographs. Two photon-counting micro-channel-plate detectors with KBr photocathodes image the dispersed light. Two of the optical systems use LiF coatings and produce spectra covering the $\sim$ 990–1187 Å wavelength range. The other two systems use SiC coatings on the optics to provide spectral coverage down to 905 Å. Our observations of Ton S180 used the $30'' \times 30''$ low-resolution apertures. We obtained good spectra from the LiF1 and LiF2 channels covering the 987–1187 Å band, and lower signal-to-noise-ratio (S/N) spectra from the SiC1 and SiC2 channels covering 905–1091 Å. The flux scale is accurate to $\sim$10 %, and the wavelength scale is accurate to $\sim$15 km s^{-1}. For detailed analysis of line and continuum fluxes, we bin this spectrum by 5 pixels, preserving the $\sim$ 20 km s^{-1} resolution of this observation. Figure 1 shows that while the *FUSE* observation was not performed simultaneous with *Chandra* it does cover a similar mean flux state to that covered by the *Chandra* observation.

6.2. FUSE Results

As seen in Figure 4, the far-UV spectrum of Ton S180 shows a bright, blue continuum and prominent broad O VI emission. Fainter emission from S VI $\lambda\lambda$934, 945, C III λ977, N III λ991, and He II λ1085 may also be present. The foreground Galactic and intergalactic

absorption visible in this spectrum has already been discussed by Savage et al. (2000), Sembach et al. (2000), and Shull et al. (2000), one noteworthy feature is the deep absorption by Lyβ. In addition to these foreground features, absorption at three velocities near the redshift of Ton S180 is visible in the O VI $\lambda\lambda$1032,1038 resonance doublet (Figure 4).

To measure the strengths of these features and that of the broad O VI emission, we used the IRAF task `specfit` (Kriss 1994). We used a power law for the underlying local continuum, a broad Gaussian for each of the O VI emission lines with their fluxes fixed at a 2:1 ratio, and Gaussians for the narrow absorption lines. The broad O VI lines have a full-width at half maximum (FWHM) of 2600 ± 186 km s^{-1} and a total flux of $(1.10 \pm 0.05) \times 10^{-12}$ ergs s^{-1} cm^{-2}. They are blueshifted relative to the systemic redshift by 490 ± 69 km s^{-1}. Unfortunately, the Lyβ lines corresponding to these velocities fall in the gaps between the LiF detector segments, and so we must use the lower S/N SiC2A data to measure their strengths. No Lyβ lines are detected.

For the O VI absorption lines the measured equivalent widths (W_λ) column densities and full-widths at half maximum (FWHM) are summarized in Table 2. The doublets have optical depths consistent with a 2:1 ratio, implying full coverage of the underlying continuum and broad emission lines. Given the strength of the O VI absorption and the weakness of any corresponding neutral hydrogen, we conclude that this gas is in a fairly high state of ionization.

7. HST

7.1. STIS Data Reduction

As *HST* was in safe-mode during 1999 December the earliest we could obtain *HST*/STIS observations of Ton S180 was 2000 January 22 (UT). We used the 52″x 0.″2 slit to obtain a UV spectrum over the range 1150–3150 Å at a spectral resolving power of $\lambda/\Delta\lambda \sim 1000$. The exposure times were 1260 s for the G140L grating and 720 s for the G230L grating. We reduced the spectra with the IDL software developed at NASA/GSFC for use by the STIS Instrument Definition Team (Lindler 1998). We then combined the G140L and G230L spectra in the region of overlap for display purposes.

7.2. STIS Results

Figure 5 shows the STIS spectrum of Ton S180. The underlying continuum form is the primary objective of this study, and to this end, we first fit simple power-law models to the STIS data, absorbed by E(B-V)=0.0296, the extinction due to Galactic material in the line-of-sight. The best-fitting power-law has slope $\alpha = 0.66 \pm 0.14$. The extrapolation of this continuum slope provides a good fit to the *FUSE* continuum, after correction of the *FUSE* data for absorption (using reddening curves from Hutchings & Giasson 2001 and Clayton et al. 1996). However, the source continuum level in the STIS data is lower than that observed in Dec 1999 by *FUSE*. We find the normalizations of the STIS and *FUSE* datasets show a flux discrepancy, in the sense that the STIS data find the source at 55% of the flux level observed by *FUSE*.

The uncertainty on absolute flux is $\sim 10\%$ for *FUSE* and $\sim 2\%$ for STIS data. Thus we attribute the discrepancy to variability in Ton S180 over the ~ 5 weeks separating those observations. Figure 1 shows that the *FUSE* observation covered a similar flux state to the *Chandra* observation, so we do not want to rescale the *FUSE* data as it samples the same flux state as the X-ray data. Given an expectation of lags between emission in the different wavelength regimes of an AGN, it is always difficult to assess how to construct the most meaningful and instructive SED. The flux discrepancy in data from the overlaping bandpass of the STIS and *FUSE* data remove ambiguities as to breaks in intrinsic spectral shape, thus for construction of the SED of Ton S180 we scaled-up the STIS and ground-based data by a factor 1.78 to compensate for the flux variability.

The absorbed powerlaw continuum extrapolates from the STIS band to agree with the *FUSE* continuum form. No spectral turnover is evident in these data, indicating that if the BBB component is contributing to the *FUSE* data, then its peak lies above ~ 912 Å (15 eV). The excesses above the continuum fit are due to known emission features which are detailed in Table 3 and some weak absorption features are also evident. In addition to the distinct lines there is evidence for emission from Fe II and Fe III between 1900 and 2300 Å similar to that observed in another NLSy1, I ZW 1 (Vestergaard & Wilkes 2001). Examination of the detailed STIS data shows that all of the emission lines expected for a Seyfert 1 galaxy are present, as well as a number of absorption lines from our Galaxy. The UV emission lines are narrow compared to those in typical Seyfert 1 galaxies; for example, the full-width at half-maximum of the C IV λ1549 Å line is $\sim 2300 \pm 80$ km s^{-1}. The peak of C IV is blueshifted by 510 ± 20 km s^{-1} with respect to the systemic velocity. The emission lines are somewhat asymmetric, as illustrated by the C IV line, with more emission in the blue wing than red wing. There is no evidence for intrinsic UV absorption lines, which occur in $\sim$60 % of normal and narrow-line Seyfert 1 galaxies (Crenshaw et al. 1999). Although we cannot

rule out the possibility of weak absorption at this resolution, we estimate an upper limit on the equivalent width of any C IV absorption to be 0.3 Å.

8. Ground-based Data

8.1. *uvby* Photometry

Strömgren *uvby* observations (Strömgren 1956) were made of Ton S180 with the Danish 1.5m telescope at ESO, La Silla, on the night of 2000 January 20-21. Observations of two secondary standards (DM-261339 and DM-38022) were also made. Each standard was observed twice in a *uvbyybvu* sequence before and after the single observation, *uvby*, of Ton S180. Each image was pre-reduced in the same standard manner. The bias, calculated as the mean of the overscan region, was subtracted and then the image was flat-fielded using the adopted sky-flat for the observing run. Instrumental magnitudes were extracted from the images using DAOPHOTII. Simple aperture photometry is all that is required since neither the standard stars nor Ton S180 reside in crowded fields. A 25.″0 (32.05 pixel) aperture was adopted. The sky background was estimated using an annulus with inner and outer radii of 64.″1 (50 pixels) and 70.″5 (55 pixels). For all the *uvby* photometry discussed here, atmospheric extinction corrections were made based on extinction coefficients determined at the Danish-50 cm telescope. On the night of these observations the extinction was marginally higher than the mean while the rms residuals between observed and catalogue indices of standard stars are a factor 3–7 larger than on nights of excellent photometric quality.

Transformations have been determined between instrumental and standard systems based upon 170 Strömgren *uvby* measurements of 42 secondary standard stars (observed in 1999, January, February, November and December). We transformed the Ton S180 instrumental photometry to the standard system, based upon the December standard transformation relations. Correcting for time-evolution of the relation, and for the difference in b filter used for the target, versus that used for the standard stars we obtain the following Strömgren magnitudes and indices for Ton S180: $u = 14.94 \pm 0.03$ mag, $v = 15.03 \pm 0.02$ mag, $b = 14.74 \pm 0.02$ mag, $y = V = 14.58 \pm 0.02$ mag, $(b - y) = 0.16 \pm 0.02$ mag and $c_1 = -0.380 \pm 0.04$ mag. To take into account the various possible error sources deriving from a) the use of a different b filter and b) the zero-point offsets, we have adopted uncertainties of twice the rms residuals for the full 1999 standard star dataset.

We convert *uvby* magnitudes into monochromatic fluxes via the equation $f_\lambda = 10^{m_\lambda/-2.5} F_{\lambda,m_\lambda} = 0$ where the calibrating fluxes F_{λ,m_λ} are taken from Pritchard et al. (1998). The fluxes obtained are listed in Table 4. The errors on fluxes are propagated from those on the magni-

tudes.

8.2. Infrared Photometry

On 2000 Jan. 23 (JD 2451567.54) we observed Ton S180 with the near-IR imager/spectrograph OSIRIS mounted on the CTIO 1.5 m telescope. A total of 300 s in K', and 150 s in both J and H were recorded for Ton S180 along with the standard star 9103 (Persson et al. 1998). The standard star is located in the vicinity of Ton S180 at a similar airmass. The instrumental magnitudes were transformed to the system of Persson et al. (1998) based on the offsets found for the standard star. This gave $J = 13.22 \pm 0.04$ mag, $H = 12.60 \pm 0.03$ mag, and $K_s = 11.67 \pm 0.03$ mag where the errors are random errors from photometry and zero points. The calibration was checked against another standard observed about an hour later at a similar airmass, yielding good agreement.

To convert the magnitudes to monochromatic fluxes we use the J and H zero magnitude fluxes computed by Cohen et al. (1992) which are based on Kurucz models of Vega and Sirius. These models are computed for the UKIRT system (Casali & Hawarden 1992) but Persson et al. (1998) show that their magnitudes have a similar zero point. For the K_s zero magnitude flux we adopt the value from Tokunaga (1997) quoted in the OSIRIS users manual. The resulting monochromatic fluxes, f_λ, computed as in the previous section are given in Table 4.

9. Examination of the SED

First we compared the SED data to the power-law continua determined for the UV and X-ray regimes. Figure 6 shows the extrapolation of the best-fitting power-law to the *HST*/STIS data ($\alpha = 0.66$) greatly overpredicts the X-ray flux. Clearly the spectrum must break somewhere between the UV and soft X-ray regimes. Also shown is the hard X-ray continuum slope, $\alpha = 1.44$, extrapolated to lower energies. This continuum intercepts the UV data around a few thousand Å but again, the hard X-ray power-law must terminate somewhere between the UV and soft X-ray regimes, as it overpredicts the optical and infrared data.

In order to examine the approximate energy distribution for Ton S180 we first corrected the data for the small amount of extinction due to the Galactic line-of-sight gas. In the STIS band the reddening correction was made following Cardelli, Clayton & Mathis (1989) and in the *FUSE* band using Hutchings & Giasson (2001) and Clayton et al. (1996), both assuming E(B-V)=0.0296, the Galactic extinction. The absorption correction in the X-

ray regime was made following Morrison & McCammon (1983) and assuming a Galactic value $1.55 \times 10^{20}\mathrm{cm}^{-2}$. Table 6 summarizes some useful data from the SED. A simple parameterization was made of the spectral shape using the hard X-ray power-law, $\alpha = 1.44$ breaking to $\alpha = 2.5$ at 1 keV and then breaking to $\alpha = 0.66$ at 0.1 keV. This parameterization is shown as a solid green line in Figure 7. The peak of the SED in this case is 80 eV. The dotted green lines denote the uncertainty in the intrinsic SED, due to some uncertainty in the line-of-sight absorption measurement. Parameterization of the soft X-ray regime as a steep power-law is clearly inadequate, and we also overlay an alternative model with continuum plus DISKBB soft component. It is interesting to see that the best-fitting DISKBB model, which has a temperature of 98 eV at the inner radius, does not predict any BBB component would appear in the UV band.

Even application of the physically meaningful models such as DISKBB leave some unmodeled structure in the soft component, i.e. a sharp spectral break below 0.3 keV. It is currently unclear whether this structure represents the intrinsic form of the soft X-ray emission or whether it represents a residual uncertainty in the ACIS/LETG calibration. The break is not well modeled using neutral or ionized gas. The most obvious possibility remaining is that this sharp feature is due to the presence of emission features. However, uncertainty in calibration prompts us to note this structure but not to model it in detail.

10. Discussion

10.1. Interband Indices

Table 7 shows the indices between various wavebands for Ton S180, compared to some values previously determined for other Seyfert type galaxies. A commonly cited slope is α_{ox}, and the value $\alpha_{\mathrm{ox}} = 1.52 \pm 0.02$ derived for Ton S180 is consistent with $\alpha_{\mathrm{ox}} = 1.46^{+0.05}_{-0.07}$ found for a sample of optically-selected radio quiet AGNs (Zamorani et al. 1981). Ton S180 appears X-ray weak compared to the mean index of 1.14 ± 0.18 determined for the *ROSAT* International X-ray/Optical Survey (RIXOS, Puchnarewicz et al. 1996) however, Ton S180 does lie within the the broad range found for RIXOS sources, which include both BLSy1s and NLSy1s. The value $\alpha_{\mathrm{ox-hard}}$ was defined in Grupe et al. (1998) as the index linking 5500 Å and 1 keV, and Ton S180 lies within the broad ranges found for soft X-ray and hard X-ray selected AGN from that study, based on *ROSAT* observations.

There are two questions of interest here, one is whether NLSy1s as a class have systematically different interband indices to BLSy1s, and the other is whether Ton S180 is unusual compared to other NLSy1s. Nagao et al. (2001) have broached the first question by

comparing the quantity α_{ox} for NLSy1s and BLSy1s. Those authors find average values and 1σ deviations $\alpha_{ox-NLSy1} = 1.31 \pm 0.16$ and $\alpha_{ox-BLSy1} = 1.36 \pm 0.24$, thus concluding there to be no significant differences between this quantity for the two extremes of the Seyfert 1 population, contrary to some previous results (**?**, e.g.)]puch96.

In summary, based upon the comparison of interband indices with other studies yields no evidence that Ton S180 has an unusual ratio of optical/UV to X-ray flux. While opinions in the literature differ on whether there is a systematic difference in α_{ox} for the extremes of the Seyfert 1 population, it seems clear that interband indices have large ranges and their use is best suited to comparison of large samples of sources. In this study we proceed by more detailed examination of the shape of the SED, and comparison of our data with other detailed SEDs.

10.2. The Form of the SED

A SED for Ton S180 was first presented by Comastri et al. (1998), who found the soft X-ray component to contain the bulk of the energy in this Seyfert galaxy. This campaign of observations provides a more complete SED for Ton S180 than previously available, with a large amount of simultaneous data.

Examination of the detailed energy distribution of Ton S180 reveals significant differences compared to some other well-studied AGN. Figure 7 shows the extinction-corrected SED of Ton S180, and some parameterizations of its form. Overlaid on the parameterizations of the SED of Ton S180 are the SEDs of other AGN; NGC 5548 is shown as a magenta dash-dotted line (Kraemer et al. 1998) while the mean radio-loud and radio-quiet quasars (from Elvis et al. 1994) are shown as dotted black and dashed blue lines, respectively. The most immediate result is that the SEDs of the Seyfert galaxies appear to peak somewhere in the extreme UV/soft X-ray band, while the quasars peak in the UV regime. Furthermore, the SED of Ton S180 peaks at a higher energy than that of NGC 5548.

Some caution is required in the comparison of SEDs constructed with different datasets and various assumptions. Some apparent difference in SEDs could be an artifact of the assumption of some continuum form for the quasars, versus a simple joining of the soft X-ray to UV data for the Seyferts. However, such assumptions are only necessary in the problematic regime between ~ 900Å and ~ 0.1 keV. We find the evidence for true underlying differences between Ton S180 and the comparison sources to be strengthened by the absence of a contribution from the BBB in the UV band of Ton S180.

A standard optically thick, geometrically thin accretion disk (Shakura & Sunyaev 1973)

predicts the temperature of the peak of the disk spectrum $T(R)$ to be a function of the mass of the central black hole and the accretion rate: $T(R) \sim 6.3{\times}10^5\ (\dot{M}/\dot{M}_{\rm Edd})^{1/4}\ M_8^{-1/4}\ (R/R_{\rm S})^{-3/4}$K (Peterson et al. 2000), where R is the radius, $R_{\rm S}$ is the Schwarzschild radius, M_8 is the mass in units of $10^8 M_\odot$ and $\dot{M}$ is the accretion rate in units of the Eddington accretion rate. All other things being equal, a difference of two orders of magnitude in mass should yield a disk spectrum whose peak energy is a factor of 3 lower for the higher-mass system than the lower-mass system; similarly, a factor 100 increase in accretion rate (relative to the Eddington rate) shifts the peak to a factor 3 higher energy. Thus the RQQ SED (Figure 8) represents sources radiating at substantially below the Eddington accretion rate, and having a high central mass; these yield a relatively cool disk spectrum. At the other extreme, NLSy1s are thought to be accreting close to the Eddington limit, and have a low mass; the disk spectrum appears hot. The BLSy1 NGC 5548 represents an intermediate system in terms both of the accretion rate and central mass, and this appears to have an intermediate SED. Telfer et al. (2002) find that for a sample of QSOs, the entire continuum from 10 eV to 2 keV can be represented by a single power-law; this is clearly not the case in Ton S180 where the X-ray spectrum steepens below 2 keV, and neither the soft or hard X-ray components extrapolate to meet the UV data in a satisfactory way[16].

NGC 5548 has a central black hole mass estimated at $\sim 10^8 M_\odot$ (Kaspi et al. 2000). If the peak of the SED for NGC 5548 is close to the Lyman limit ($T \sim 1.6 \times 10^5$K) then an accretion rate of 11% of Eddington would be estimated, assuming a standard thin disk picture.

Few strong constraints exist on the central mass in Ton S180. From variability observed in the X-ray regime Romano et al. (2002) found $M_{\rm BH} \gtrsim 8 \times 10^6 M_\odot$ for Ton S180; however, those authors assumed a bolometric luminosity which is lower than that revealed by this SED, leading to a revised limit $M_{\rm BH} \gtrsim 8 \times 10^7 M_\odot$. Mass estimates such as these can be misleading if the X-ray variability is due, for example, to flares on the surface of the accretion disk, as the timescale of variation may not be directly related to the scale-size of the disk system. Thus we examine an alternative estimate of mass based upon the luminosity at 5100 Å ($\nu L_\nu \sim 3 \times 10^{44}$erg s^{-1}). Using the relation derived from other NLSy1s (Peterson et al. 2000, their Figure 7) we estimate a central mass $M \sim 2 \times 10^7 M_\odot$ (with a factor ~ 2 uncertainty) and the broad line region to exist at a radius ~ 100 light days (Peterson et al. 2000, their Figure 6). This is in keeping with the systematically large BLR radii suggested by Giannuzzo

[16]While the *Chandra* data show a turnover at 0.3 keV, this turnover is sharper than that expected from observation of the peak of the disk spectrum and there is some discrepancy between these data and data from other instruments. For these reasons, henceforth we will assume this turnover does not indicate the peak temperature of the disk.

& Stirpe (1996) for NLSy1s compared to BLSy1s. As the level of starlight contamination of the 5100 Å flux is difficult to assess, this mass should be considered as an upper limit on the true central mass. The difference in SED peak energies is thus expected, as Ton S180 has a lower mass than NGC 5548, and NLSy1s are thought to have systematically higher accretion rates than BLSy1s.

Unfortunately, the peak of the spectrum in Ton S180 remains loosely constrained. The *EUVE* data favor the simple parameterization of the XUV spectrum (Figure 7) indicating that the peak lies close to or below 100 eV. Assuming a standard disk spectrum, the disk temperature must be greater than $\sim 15\,\mathrm{eV}$, the peak of any cooler component of significant flux would show up in the *FUSE* data. The SED data indicate a peak close to 100 eV. Assuming a peak in disk emission for Ton S180 at this energy, which corresponds to $4\times10^5\,\mathrm{K}$, then for $M \sim 2 \times 10^7 M_\odot$, $\dot{M} \sim 0.88 \times \dot{M}_{\rm Edd}$. For black holes operating near the Eddington limit the accretion disk surface is predicted to be highly ionized. There is certainly strong evidence for an ionized disk in Ton S180, as the Fe Kα line appears to be produced in highly ionized material in *BeppoSAX* (Comastri et al. 1998) and *ASCA* data (Turner, George, & Nandra 1998).

The results from Ton S180 appear to fit into the standard disk picture. However, we also note that Cheng, Gaskell & Koratkar (1991) conclude that the standard disk model is not applicable to the UV spectra of quasars. Their case rests on the lack of any relation between $\alpha_{\rm uv}$ and luminosity. However, since the peak of the disk spectrum is generally at rest wavelengths of 1000 Å or shorter (Zheng et al. 1997; Telfer et al. 2002), α_{uv} is indicative of only the rising edge of the disk spectrum. In the standard disk model, the spectral slope in this region is relatively insensitive to luminosity, so one does not necessarily expect a strong correlation between α_{uv} and luminosity of the BBB.

As a final note, the lowest frequency IR point lies above the adjacent IR points. This has been observed in many AGN and is due to thermal emission from dust grains heated to close to their evaporation temperature (1500 K for graphite) close to the central engine (Rieke 1978). Recently, strong near-IR emission from the Seyfert 1 galaxy NGC 7469 has been attributed to very hot dust grains ($T > 900$ K) associated with the putative torus (Marco & Alloin 1998), this is also observed in the SED of NGC3783 (Alloin et al. 1995).

10.3. The Energy Budget of Ton S180

The multi-power-law parameterization of the SED for Ton S180 makes it possible to estimate the luminosity in various energy regimes, helping to constrain reprocessing mech-

anisms and isolate the primary energy source. Table 8 shows the observed and intrinsic luminosities in several energy-bands, defined in the rest-frame of the source. The implied bolometric luminosity is $L_{bol} \sim 10^{46}$ erg s^{-1}. More luminosity emerges in the 10 - 100 eV regime than the 100 eV to 10 keV regime. Assuming that we are seeing all emitted radiation in each wavelength regime then this indicates that the EUVE–soft X-ray band contains the primary spectral component, in keeping with disk-corona models (e.g. Haardt & Maraschi 1991).

The energy budget and the SED show that Ton S180 is relatively X-ray weak above ~ 2 keV (interband indices are insensitive to this, as historically X-ray fluxes for comparison with optical fluxes have been taken at soft X-ray energies). One possible reason for this is Compton-cooling of the hard spectrum by the large flux of soft X-ray and UV photons, as discussed by many authors, including Pounds, Done, & Osborne (1995).

10.4. The State of the Circumnuclear Gas

The weak O VI absorption features detected in the *FUSE* data, the absence of absorption from lower ionization species in the *HST* data, and the lack of detectable X-ray absorption in the *Chandra* spectrum together indicate the presence of a small column of circumnuclear material which appears to be in a high state of ionization compared to that observed in other well-studied sources such as NGC 5548 and NGC 3783. The outflow velocity of ~ 500 km s^{-1} is not unusual. Many Seyfert galaxies have shown evidence for outflow in UV and optical data (e.g. Crenshaw et al. 1997). In the X-ray regime *Chandra* grating observations have revealed supporting evidence for outflowing gas, with velocities of order a few hundred km s^{-1} (e.g. Collinge et al. 2001; Kaastra et al. 2000; Kaspi et al. 2000, 2001). A picture of Ton S180 being shrouded by highly ionized gas is consistent with earlier BeppoSAX (Comastri et al. 1998) and *ASCA* (Turner, George, & Nandra 1998) observations of Fe Kα emission, as well as the new *ASCA* data which show that the narrow component of Fe Kα is consistent with emission from Fe XXV–Fe XXVI.

The ratio of the O VI to H I absorbing columns in the UV regime is comparable to that of the high-ionization component detected in Mrk 509 (Kriss et al. 2000), which was tentatively identified with the X-ray warm absorber in that object. However, in Ton S180 the total equivalent column density of hydrogen associated with the UV absorber must be $< 10^{17}$ cm^{-2}; too low to produce detectable X-ray absorption. However, the absence of ionized circumnuclear gas does not appear to be a general property of NLSy1s. Some NLSy1s do appear to show signatures of a warm absorber in the X-ray regime (**?**, e.g.)]Lee01,Collea01 as well as UV absorption systems (Crenshaw et al. 1999).

To examine the relation between the ionizing spectrum in Ton S180 and the circumnuclear gas, we took two estimates of the SED and total ionizing flux. The conservative estimate links the softest X-ray point at ~ 0.3 keV to the highest end of the UV data with a simple power-law. For this SED, the total luminosity from 0.01 - 10 keV is $\sim 2.0 \times 10^{45}$ ergs s^{-1} and the corresponding luminosity in ionizing photons is Q $\sim 2.9 \times 10^{55}$ photons s^{-1}. Taking instead the (extreme) SED that peaks in the EUV (green line in Figure 7), the 0.01 – 10 keV luminosity is $\sim 3.8 \times 10^{45}$ erg s^{-1} and Q $\sim 4.5 \times 10^{55}$ photons s^{-1}.

Assuming the typical density and ionization parameter in the optical broad-line region (BLR) clouds, the radii at which the BLR exists can be estimated. Wandel, Peterson & Malkan (1999) used these "photoionization radii" and the measured line widths to derive black hole masses, which were in general agreement with those determined via reverberation mapping. In order to explore the role of luminosity on the line widths we instead use the masses derived from reverberation mapping and the photoionization radii (r) to estimate the line widths. Following Wandel, Peterson & Malkan (1999), we assume $Q/(4\pi r^2 c\ n_e) \times n_e \sim 10^{10}$ for the line emitting gas. Based on our estimates of the ionizing luminosity of the central source in Ton S180, we derive representative radial distances of r $\sim 8.8 \times 10^{16}$ cm and $\sim 1.1 \times 10^{17}$ cm, for the conservative and extreme cases, respectively (~ 40 light days, somewhat smaller than the radius estimated from Peterson et al. 2000). If the BLR clouds are virialized around the central black hole, the FWHM of the emission lines should be roughly equal to $\sqrt{GM/r}$; for a black hole mass of $10^7 M_\odot$, FWHM $\sim$ 1290 km s^{-1} (conservative case) and 1160 km s^{-1} (extreme case), in reasonable agreement with the observed FWHM of Hβ.

We have estimated the total ionizing flux, Q, for two BLSy1's: for NGC 4151, Q is $\sim$ 2–8 $\times 10^{53}$ photons s^{-1} (Kraemer et al. 2001); for NGC 5548, Q is $\sim 1 \times 10^{54}$ photons s^{-1} (Kraemer et al. 1998). Assuming the black hole masses quoted by Wandel, Peterson & Malkan (1999) (1.2 x $10^7 M_\odot$ for NGC 4151, and 6.8 x $10^7 M_\odot$ for NGC 5548), the corresponding "typical" BLR cloud distances and velocities are r $\sim 1.2 \times 10^{16}$ cm and FWHM $\sim$ 3700 km s^{-1} for NGC 4151, and r $\sim 1.6 \times 10^{16}$ cm and FWHM $\sim$ 7460 km s^{-1} for NGC 5548; the FHWMs are in rough agreement with the observed values. Clearly, the narrowness of the emission lines in Ton S180 is partially due to its stronger ionizing flux. Furthermore, given these "typical" BLR conditions, it is likely that the clouds within a few light days of the central source are too highly ionized even to produce much C IV emission (for a discussion of range in conditions in which emission lines form, see Baldwin et al. 1995). Hence, the higher value of Q for Ton S180 requires that the BLR gas is either more highly ionized than in BLSy1s or, if the emission-line ratios are the same, it must be denser (i.e., denser gas is now ionized enough to contribute significantly to the emission-line spectrum). Either way, conditions are not identical to those in typical BLSy1s.

11. Summary

Construction of the spectral energy distribution for the bright NLSy1 galaxy Ton S180 shows that most of the energy is emitted in the 10 – 100 eV regime, indicating that the primary source of emission dominates that band. The UV and X-ray data together constrain the peak of any BBB component to lie between 15 and 100 eV. This, and the overall shape of the SED indicate that emission from the accretion disk peaks at significantly higher energies in this source than in BLSy1s, as expected if NLSy1s have smaller central black holes and higher accretion rates. High-resolution spectra from *FUSE* reveal UV absorption due to O VI. The absence of absorption features in the *HST* data and the lack of neutral hydrogen absorption in the *FUSE* spectrum indicate a high-ionization state for the absorbing gas, while the absence of soft X-ray absorption that shows that the column density is quite low. The highly-ionized state of the circumnuclear gas is most likely linked to the high luminosity and steep slope of the ionizing continuum in Ton S180. Given our constraints on the SED in Ton S180, we find that typical BLR emission lines would form at a radius which is an order of magnitude further out than in typical BLSy1s. The BLR is estimated to exist at a radius $\sim 10^{17}$ cm, or 40 light days.

12. Acknowledgements

We are grateful to the satellite operation teams for co-ordination of the multi-waveband observations. This research has made use of the NASA/IPAC Extragalactic database, which is operated by the Jet Propulsion Laboratory, Caltech, under contract with NASA; of the Simbad database, operated at CDS, Strasbourg, France; and data obtained through the HEASARC on-line service, provided by NASA/GSFC. This work is based in part on data obtained for the Guaranteed Time Team by the NASA-CNES-CSA *FUSE* mission operated by the Johns Hopkins University. Financial support to U. S. participants has been provided by NASA contract NAS5-32985. T.J. Turner, G. Kriss, S. Mathur and P. Romano acknowledge support from NASA grants NAG5-7538, NAGW-4443, NAG5-8913 and NAG5-9346 respectively. This research was supported by the Danish Natural Science Research Council through its Centre for Ground-Based Observational Astronomy. Funding for the OSIRIS instrument was provided by grants from The Ohio State University, and National Science Foundation Grants AST-9016112 and AST-9218449. The 1.5 m telescope at CTIO is operated by the Association of Universities for Research in Astronomy Inc. (AURA), under a cooperative agreement with the NSF as part of the National Optical Astronomy Observatories (NOAO). We thank the anonymous referee for useful comments.

REFERENCES

Alloin, D., et. al. 1995, A&A, 293, 293

Baldwin, J., Ferland, G., Korista, K., Verner, D. 1995, ApJ, 455, L119

Ballantyne, D. R., Iwasawa, K., & Fabian, A. C. 2001, MNRAS, 323, 506

Boller, Th., Brandt, W. N., & Fink, H. 1996, A&A, 305, 53

Boller, Th., Fabian, A.C., Sunyaev, R., Trümper, J., Vaughan, S., Ballantyne, D.R., Brandt, W.N., Keil, R., Iwasawa, K. 2001 (astro-ph/0110367)

Brandt, W. N., Fabian, A. C., Nandra, K., Reynolds, C. S., & Brinkmann, W. 1994, MNRAS, 271, 958

Branduardi-Raymont, G., Sako, M., Kahn, S. M., Brinkman, A. C., Kaastra, J. S., & Page, M. J. 2001, A&A, 365, L140

Brandt, W. N., Mathur, S., & Elvis, M. 1997, MNRAS, 285, L25

Cardelli, J. A., Clayton, G. C., Mathis, J. S. 1989, ApJ, 345, 245,

Casali, M. M., & Hawarden, 1992, JCMT-UKIRT Newsletter, 4, 33

Cheng, F. H., Gaskell, C. M., Koratkar, A. P. 1991, ApJ, 370, 487

Clayton, G. C., et al. 1996, ApJ, 460, 313

Cohen, M., Walker, R. G., Barlow, M. J., & Deacon, J. R. 1992, AJ, 104, 1650

Collinge, M. J. et al. 2001, ApJ, 557, 2

Comastri, A., et al. 1998, A&A, 333, 31

Comastri, A., et al. 2001, A&A, 365, 400

Crenshaw, D. M., Kraemer, S. B., Boggess, A., Maran, S. P., Mushotzky, R. F., & Wu, C. 1999, ApJ, 516, 750

Crenshaw, D. M., 1997, in ASP Conf Ser 113, Emission Lines in Active Galaxies: new Methods and Techniques, ed. B.M. Peterson, F.-Z. Cheng & A.S.Wilson, IAU Collq. 159 (San Francisco: ASP), 240

Chiang, J., Reynolds, C. S., Blaes, O. M., Nowak, M. A., Murray, N., Madejski, G., Marshall, H. L., & Magdziarz, P. 2000, ApJ, 528, 292

Davidson, K., Netzer, H. 1979, Rep. Prog. Phys., 51, 715

Dickey, J. M., Lockman, F. J., 1990, ARAA. 28, 215.

Edelson, R. & Nandra, K. 1999, ApJ, 514, 682

Edelson, R., et al. 2002, in press (astro-ph/0108387)

Elvis, M., et al. 1994, ApJS, 95, 1

Fink, H. H., Walter, R., Schartel, N., & Engels, D. 1997, A&A, 317, 25

Fiore, F., et al. 1998, MNRAS 298, 103

George, I. M., Turner, T. J., Yaqoob, T., Netzer, H., Laor, A., Mushotzky, R. F., Nandra, K., Takahashi, T. 2000, ApJ, 531, 52

Giannuzzo, M. E., Stirpe, G. M. 1996, A&A, 314, 419

Grupe, D., Beuermann, K., Thomas, H.-C., Mannheim, K., & Fink, H. H. 1998, A&A, 330, 25

Haardt, F., & Maraschi, L., 1991, ApJ, 380, 51

Hamuy, M., Walker, A. R., Suntzeff, N. B., Gigoux, P., Heathcote, S. R., & Phillips, M. M. 1992, PASP, 104, 533

Hamuy, M., Suntzeff, N. B., Heathcote, S. R., Walker, A. R., Gigoux, P., & Phillips, M. M. 1994, PASP, 106, 566

Hutchings, J. B. & Giasson, J., 2001, PASP, 113, 1205

Kaastra, J. S., Mewe, R., Liedahl, D. A., Komossa, S., & Brinkman, A. C. 2000, A&A, 354, L83

Kaspi, S. 2000, in Probing the Physics of AGNs by Multiwavelength Monitoring", Eds, B. M. Peterson, R. S. Polidan, R. W. Pogge, (San Francisco, ASP).

Kaspi, S., Brandt, W. N., Netzer, H., Sambruna, R., Chartas, G., Garmire, G. P., & Nousek, J. A. 2000, ApJ, 535, L17

Kaspi, S. et al. 2001, ApJ, 554, 216

Korista, K., Ferland, G., & Baldwin, J. 1997, ApJ, 487, 555

Kraemer, S. B.,Crenshaw, D. M., Filippenko, A. V., & Peterson, B. M. 1998, ApJ, 499, 719

Kraemer, S. B., et al. 2001, ApJ, 551, 671

Kriss, G. 1994, in ASP Conf. Ser. 61, Astronomical Data Analysis Software and Systems III, ed. D. R. Crabtree, R. J. Hanisch, & J. Barnes, 437

Kriss, G. A. et al. 2000, ApJ, 538, L17

Laor, A., Fiore, F., Elvis, M., Wilkes, B. J., McDowell, J. C. 1997, ApJ, 477, 93

Laor, A. 1998, ApJ, 505, L83

Lawrence, A., Elvis, M., Wilkes, B. J., McHardy, I., Brandt, N. 1997, MNRAS, 285, 879

Lee, J. C., Ogle, P. M., Canizares, C. R., Marshall, H. L., Schulz, N. S., Morales, R., Fabian, A. C., Iwasawa, K. 2001, ApJ, 554, 13

Leighly, K. M. 1999b, ApJS, 125, 317

Lindler, D. 1998, CALSTIS Reference Guide (CALSTIS Version 5.1)

Makishima, K., Maejima, Y., Mitsuda, K., Bradt, H. V., Remillard, R. A., Tuohy, I. R., Hoshi, R., & Nakagawa, M. 1986, ApJ, 308, 635

Malkan, M. A. & Sargent, W. L. W. 1982, ApJ, 254, 22

Marco, O., & Alloin, D. 1998, A&A, 336, 823

Mathews, W. G. & Ferland, G. J. 1987, ApJ, 323, 456

Mathur, S., Elvis, M., & Wilkes, B. 1995, ApJ, 452, 230

Matt, G., Fabian, A. C., & Ross, R. R. 1993, MNRAS, 264, 839

Matt, G., Fabian, A. C., & Ross, R. R. 1993, MNRAS, 278, 1111

Mitsuda, K., et al. 1984, PASJ, 36, 741

Moos, H. W., et al. 2000, ApJ, 538, L1

Morrison, R., & McCammon, D. 1983, ApJ, 270, 119

Nagao, T., Murayama, T., Taniguchi, Y. 2001, ApJ, 546, 744

Nandra, K., George, I. M., Mushotzky, R. F., Turner, T. J., & Yaqoob, T. 1997a, ApJ, 476, 70

Nandra, K., George, I. M., Mushotzky, R. F., Turner, T. J., & Yaqoob, T. 1997b, ApJ, 477, 602

Nowak, M. A. & Chiang, J. 2000, ApJ, 531, L13

Persson, S. E., Murphy, D. C., Krzeminski, W., Roth, M., & Rieke, M. J. 1998, AJ, 116, 2475

Peterson, B. M. et al., 2000, ApJ, 542, 161 (1st ed.; Cambridge, Cambridge University Press)

Pounds, K. A., Done, C., & Osborne, J. P. 1995, MNRAS, 277, L5

Pritchard, J. D., Tobin, W., Clark, M., & Guinan, E. F. 1998, MNRAS, 297, 278

Puchnarewicz, E. M., Mason, K. O., Romero-Colmenero, E., Carrera, F. J., Hasinger, G., McMahon, R., & Mittaz, J. P. D., Page, M. J., Carballo, R. 1996, MNRAS, 281, 1243

Rieke, G. H. 1978, ApJ, 226, 550

Romano, P., Turner, T. J., Mathur, S., & George, I. M. 2002, ApJ, 564

Sahnow, D. J., et al. 2000, ApJ, 538 L7

Savage, B. D., et al. 2000, ApJ, 538 L27

Sembach, K. R., et al. 2000, ApJ, 538 L31

Shakura, N. I., & Sunyaev, R. A. 1973, A&A, 24, 337

Shields, G. A. 1978, in Pittsburgh Conf. on BL Lac Objects, ed. A. M. Wolf, (University of Pittsburgh), 257

Shull, J. M., & Sachs, E. R. 1993, ApJ, 416, 536

Shull, J. M., et al. 2000, ApJ, 538, L73

Strömgren, B. 1956, Vistas in Astron. 2, 1336

Telfer, R.C., Zheng, W., Kriss, G.A., & Davidsen, A. F. 2002, ApJ, in press

Tokunaga, A. T. 1997, in Astrophysical Quantities, 4th Edition, editor A. Cox

Turner, T. J., et al. 1997, ApJS, 113, 23

Turner, T. J., George, I. M., & Nandra, K. 1998, ApJ, 508, 648

Turner, T. J., George, I. M., Nandra, K., & Turcan, D. 1999, ApJ, 524, 667

Turner, T. J., George, I. M., & Netzer, H. 1999, ApJ, 526, 52

Turner, T. J., et al. 1999b, in Proceedings of the 19th Texas Symposium on Relativistic Astrophysics and Cosmology, ed. J. Paul, T. Montmerle, & E. Aubourg (Saclay: CEA), E441

Turner, T. J., George, I. M., Grupe, D., Nandra, K., Remillard, R. A., Leighly, K. M., Marshall, H. L., Kraemer, S. B., & Crenshaw, D. M. 1999, ApJ, 510, 178

Turner, T. J., Perola, G. C., Fiore, F., Matt, G., George, I. M., Piro, L., & Bassani, L. 2000, ApJ, 531, 245

Turner, T. J., et al. 2001a, ApJ, 548, L13

Turner, T. J., Romano, P., George, I. M., Edelson, R., Collier, S. J., Mathur, S., & Peterson, B. M. 2001b, ApJ, 561, 131

Vaughan, S., Pounds, K. A., Reeves, J., Warwick, R., & Edelson, R. 1999a, MNRAS, 308, L34

Vaughan, S., Reeves, J., Warwick, R., & Edelson, R. 1999b, MNRAS, 309, 113

Vestergaard, M., & Wilkes, B. J. 2001, in Spectrscopic Challenges of Photoionized Plasmas. ASP Conference Series, Vol TBD, 2001, Eds. G. Ferland & D. W. Savin.

Wisotzki, A., Dreizler, S., Engels, D., Fink, H. H., & Heber, U. 1995, A&A, 297, L55

Yaqoob, T., et al. 2000, *ASCA* GOF Calibration Memo, ASCA-CAL-00-06-01, v1.0

Wandel, A., Peterson, B. M., & Malkan, M. 1999, ApJ, 526, 579

Zamorani, G., et al. 1981, ApJ, 245, 357

Zheng, W., Kriss, G. A., Telfer, R. C., Grimes, J. P., & Davidsen, A. F. 1997, ApJ, 475, 469

AAS LaTeX macros v5.0.

Table 1. Observing Log for Ton S180.

Observatory/Telescope (1)	Instrument (2)	UT Dates (3)	Notes (4)	References (5)
ASCA		1999 Dec 03–15	continuous[a]	1,2
Chandra	LETG	1999 Dec 14–15	continuous	3
RXTE[b]	PCA	1999 Nov 12–Dec 15	once every 96 min	2
EUVE		1999 Nov 12–Dec 15	continuous[a,c]	2
FUSE		1999 Dec 12	15.2 ks; 30″x 30″(LWRS)	4
HST	STIS	2000 Jan 22	6 ks; 52″x 0.″2	4
ESO 1.5m		2000 Jan 21	*uvby*	4
CTIO 1.5m	OSIRIS	2000 Jan 23	$JHKs$	4

[a]except for gaps due to Earth occultation and passage of the spacecraft through the SAA.

[b]Those data are not used in the construction of the SED, but were taken for the complementary timing project (Edelson et al. 2002).

[c]A subset of these data were used in construction of the SED.

References. — (1) Romano et al. 2002. (2) Edelson et al. 2002; (3) Turner et al. 2001a. (4) This work.

Table 2. UV Absorption Lines.

Feature	#	W_λ (Å)	$N_{\rm ion}$ ($\rm cm^{-2}$)	Δv[a] ($\rm km\ s^{-1}$)	FWHM ($\rm km\ s^{-1}$)
O VI λ 1031.93	1	0.20 ± 0.03	$1.7 \pm 0.22 \times 10^{14}$	-146 ± 15	75 ± 11
	2	0.07 ± 0.001	$6.0 \pm 0.12 \times 10^{13}$	-6 ± 15	27 ± 6
	3	0.21 ± 0.02	$2.0 \pm 0.22 \times 10^{14}$	$+109 \pm 15$	44 ± 5

[a]Velocity is relative to a systemic redshift of $z = 0.06198$.

Table 3. STIS Emission Lines.

Feature (Å)	Flux	FWHM (km s^{-1})
Lyα λ 1216	30.8 ± 6.20	1961 ± 122
N V λ 1240	7.11 ± 1.40	1700 ± 848
Si II λ 1260	0.49 ± 0.19	···
O I λ 1302	1.86 ± 0.45	921 ± 230
C II λ 1335	0.87 ± 0.30	1123 ± 280
S IV / O IV] λ 1400	4.47 ± 0.94	···
N IV] λ 1486	< 0.1	···
C IV λ 1550	8.31 ± 0.61	2300 ± 80
He II λ 1640	1.95 ± 0.78	···
O III] λ 1663	0.60 ± 0.24	···
N III] λ 1750	0.45 ± 0.22	···
Si III] λ 1892	1.25 ± 0.25	···
C III] λ 1909	2.16 ± 0.43	···
[Ne IV] λ 2324	0.24 ± 0.10	···
Mg II λ 2800	1.21 ± 0.24	1071 ± 428

[a]Observed fluxes with no absorption correction, in units 10^{-13}erg cm^{-2} s^{-1}.

Table 4. *uvby* Photometry.

Filter	λ Å	Mag.[a]	F_λ[b] (10^{-19} erg cm^{-2} s^{-1} Å^{-1})
u	3500	14.94 ± 0.03	39.75 ± 1.02
v	4110	15.03 ± 0.02	11.94 ± 0.33
b	4670	14.74 ± 0.02	7.71 ± 0.13
y	5470	14.58 ± 0.02	5.26 ± 0.09

[a]Strömgren magnitude (Strömgren 1956).

[b]No rescaling applied for source variability.

Table 5. J, H and Ks Photometry.

Filter	λ Å	Mag.	F_λ[a] (10^{-19} erg cm^{-2} s^{-1} Å^{-1})
J	12150	13.22 ± 0.04	3.45 ± 0.10
H	16540	12.60 ± 0.03	1.40 ± 0.03
Ks	21570	11.67 ± 0.03	1.14 ± 0.03

[a]No rescaling applied for source variability.

Table 6.

Rest Wavelength/Energy (keV)	νL_ν (Observed)[a]	νL_ν (Intrinsic)[a]
$2\,\mu$m	3.146	3.175
$1\,\mu$m	3.842	3.953
7000 Å	4.283	4.544
5500 Å	4.485	4.823
3000 Å	5.272	6.124
2500 Å	5.356	6.371
1000 Å	6.053	8.892
0.25 keV	1.521	3.180
1 keV	0.655	0.686
2 keV	0.307	0.313
10 keV	0.156	0.156

[a]In units of $10^{44}\,\mathrm{erg\,s^{-1}}$. $H_0 = 75$ km s^{-1} Mpc^{-1}, $q_0 = 0.5$.

Table 7. Spectral Indices

Index		Definition	Observed	Intrinsic	BLSy1
$\alpha_{3000\,\mathrm{\AA}-1000\,\mathrm{\AA}}$	$\alpha_{\rm uv}$	-2.096 $\log(F_{1000\,\mathrm{\AA}}/F_{3000\,\mathrm{\AA}})$	0.53 ± 0.14	0.66 ± 0.14	0.85 ± 0.06[a]
$\alpha_{5500\,\mathrm{\AA}-0.25\,\mathrm{keV}}$		-0.489 $\log(F_{0.25\,\mathrm{keV}}/F_{5500\,\mathrm{\AA}})$	1.24 ± 0.03	1.12 ± 0.03	0.73[b]
$\alpha_{5500\,\mathrm{\AA}-1\,\mathrm{keV}}$[c]	$\alpha_{\rm ox-hard}$	-0.378 $\log(F_{1\,\mathrm{keV}}/F_{5500\,\mathrm{\AA}})$	1.37 ± 0.02	1.38 ± 0.02	1.13 [c]
$\alpha_{1\mu\mathrm{m}-2\,\mathrm{keV}}$	$\alpha_{\rm ix}$	-0.312 $\log(F_{2\,\mathrm{keV}}/F_{1\mu})$	1.35 ± 0.02	1.35 ± 0.02	1.14-2.16 [d]
$\alpha_{2500\,\mathrm{\AA}-2\,\mathrm{keV}}$	$\alpha_{\rm ox}$	-0.384 $\log(F_{2\,\mathrm{keV}}/F_{2500\,\mathrm{\AA}})$	1.50 ± 0.02	1.52 ± 0.02	$1.46^{+0.05}_{-0.07}$ [e] 1.21 ± 0.02 [f]
α_x		-1.431 $\log(F_{2\,\mathrm{keV}}/F_{10\,\mathrm{keV}})$	1.44 ± 0.07	1.44 ± 0.07	0.91 [g]

[a] Index in the $\sim$ 2200-1200 Å band (Cheng, Gaskell & Koratkar 1991)

[b] Turner et al. 1999c.

[c] Grupe et al. 1998.

[d] Lawrence et al. 1997.

[e] Zamorani et al. 1981.

[f] Puchnarewicz et al. 1996.

[g] Nandra et al. 1997b.

Table 8. Luminosities

Energy (keV) (1)	$L_{\rm observed}$[a] (2)	$L_{\rm Intrinsic}$[a] (3)
5×10^{-4}–0.01	13.94	15.69
0.01–0.1	2.86	28.80
0.1–1	2.03	8.92
1–10	0.65	0.66
5×10^{-4}–10	19.49	54.07
0.1–10	2.69	9.57

[a]In units of $10^{44}\,{\rm erg\,s^{-1}}$.

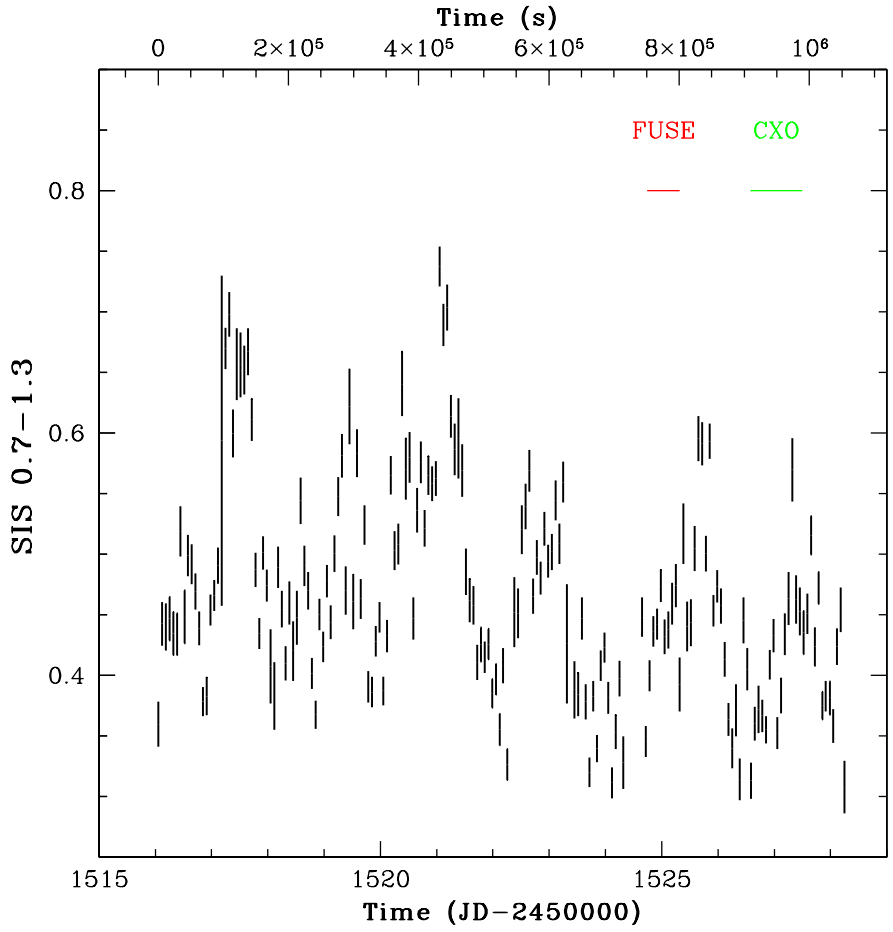

Fig. 1.— The 12-day *ASCA* light curve from Romano et al. (2002). The periods covered by *FUSE* and *Chandra* observations are noted. *EUVE* data were extracted to be simultaneous with the *Chandra* observation.

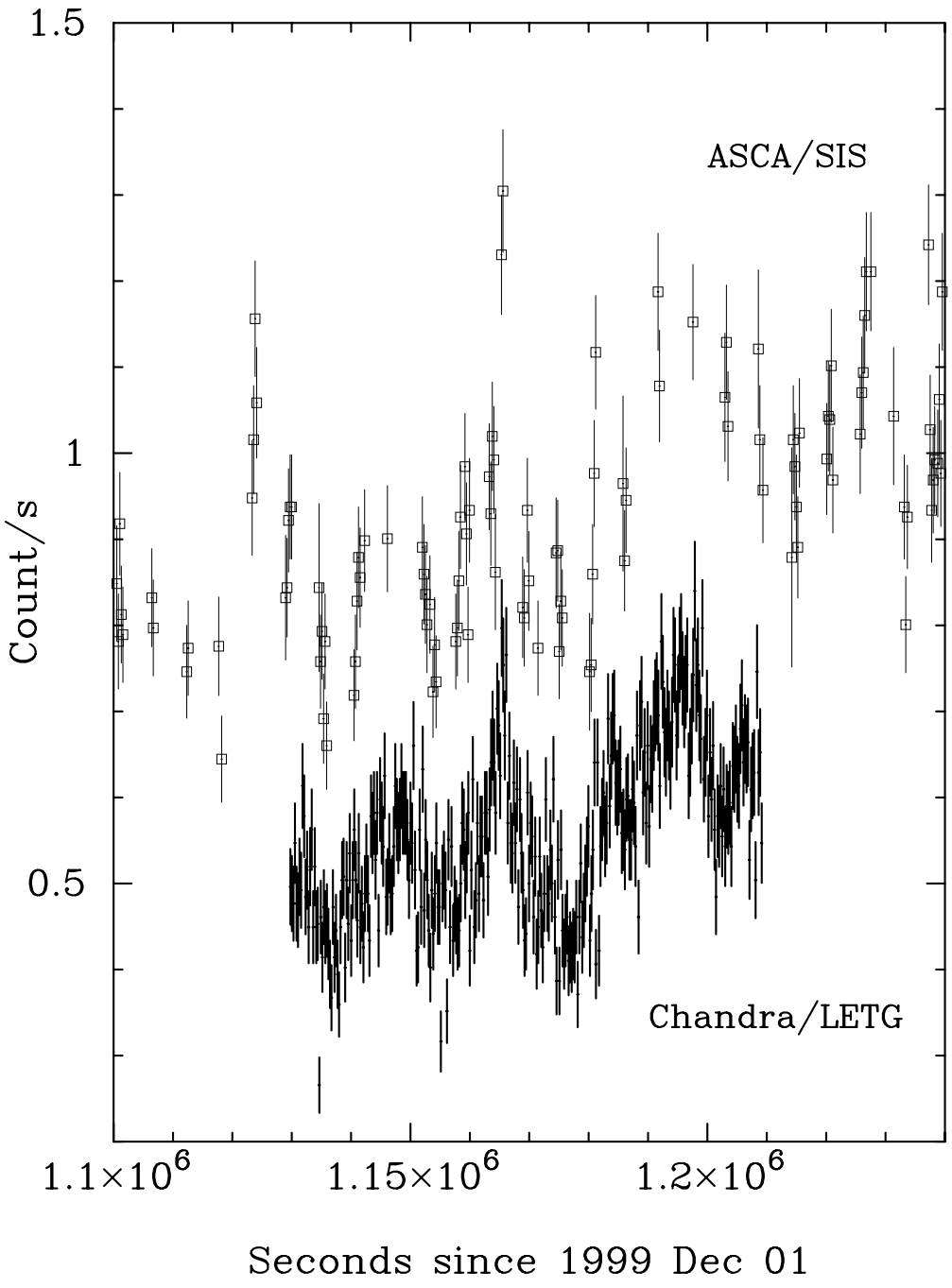

Fig. 2.— The light curve of the combined $\pm 1^{st}$ order *Chandra*/LETG data (0.2-10.0 keV) using 256 s bins. The corresponding portion of the *ASCA* SIS light curve is overlaid and denoted by the open symbols.

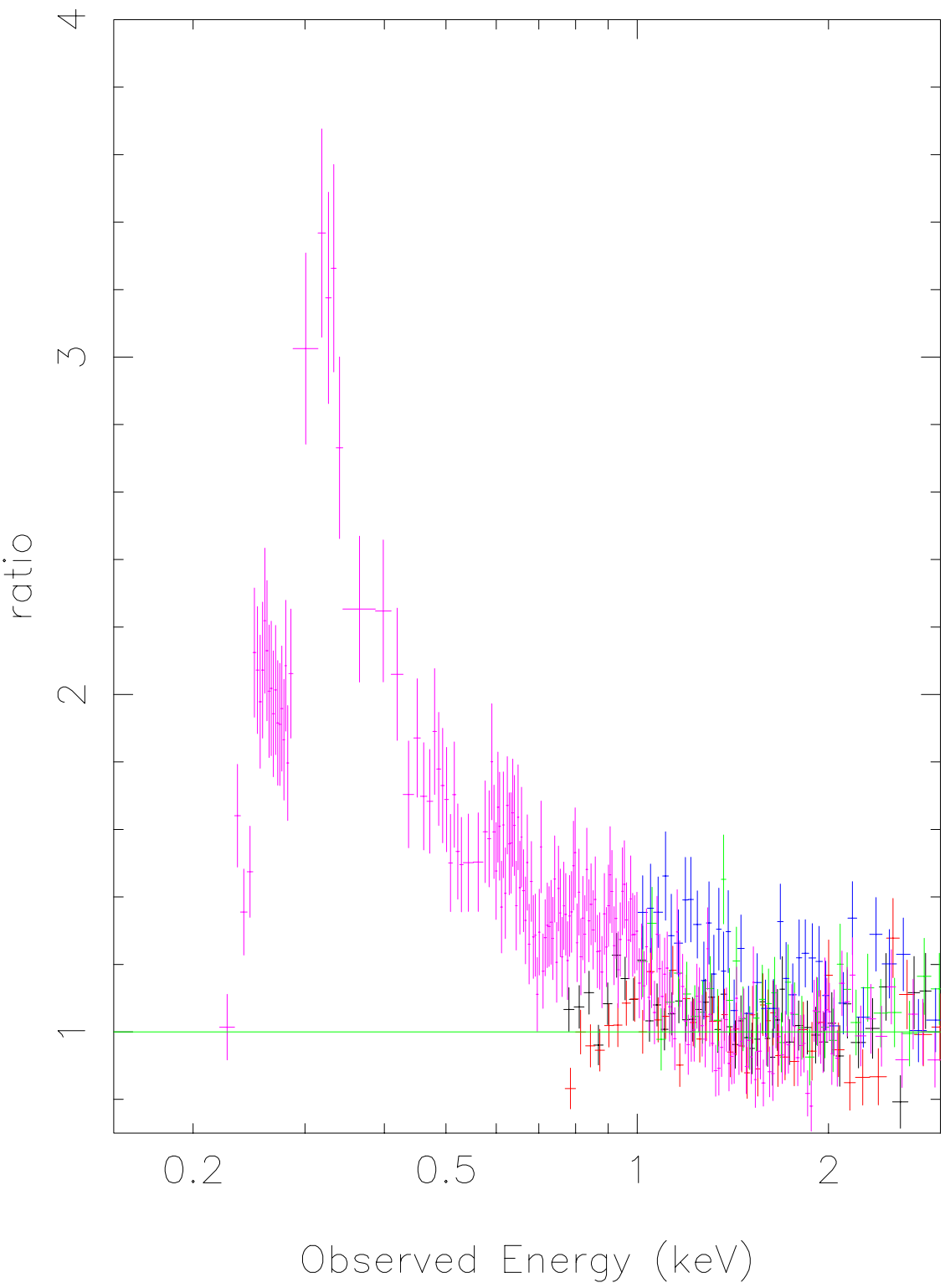

Fig. 3.— The LETG (magenta) and *ASCA* (red and black are SIS, blue and green are GIS) data/model ratio compared to the $\alpha = 1.44$ power-law. The soft excess shows a shape which may be partially due to residual calibration uncertainties below 0.3 keV.

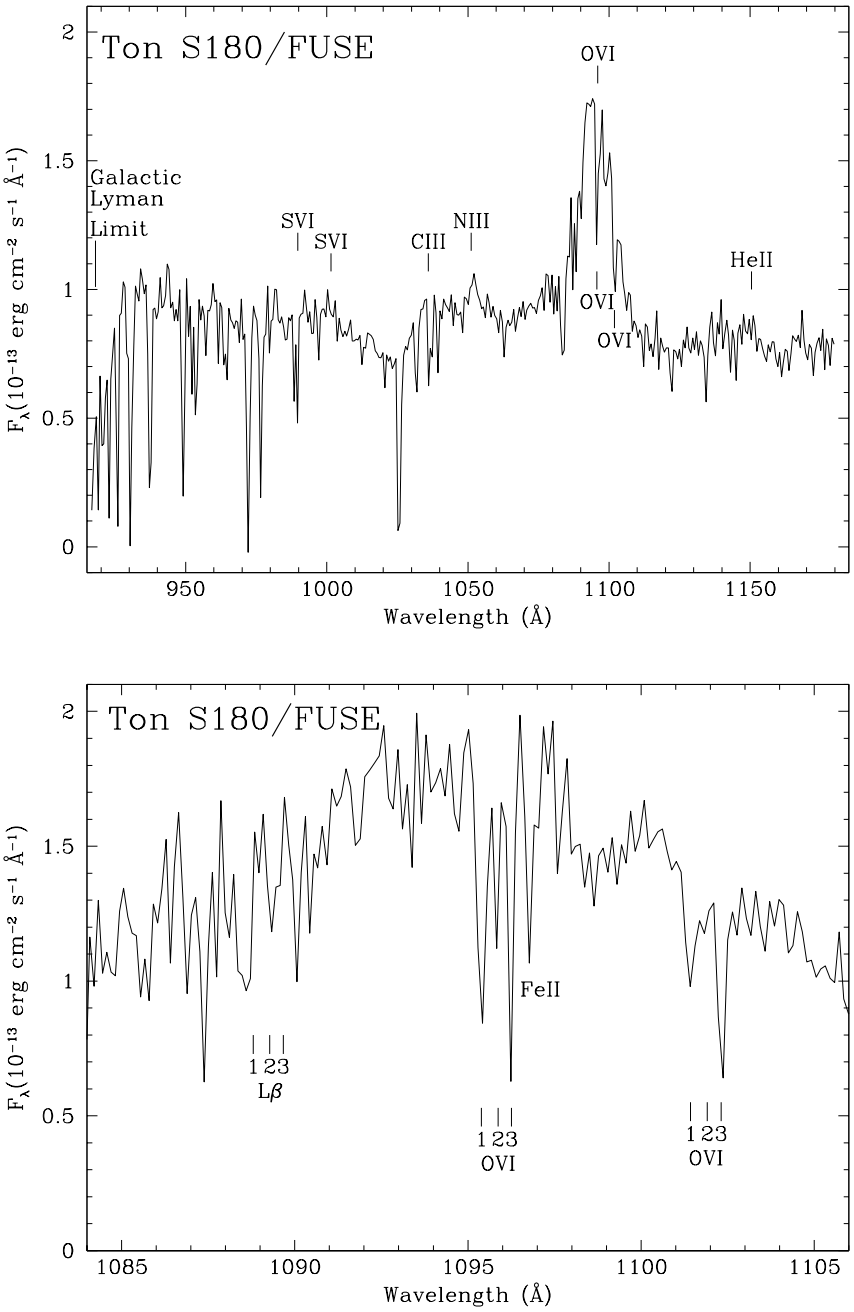

Fig. 4.— Top: *FUSE* spectrum of Ton S180 binned to a resolution of 0.6 Å (100 pixels). In addition to the noticeable broad O VI emission line, suggested identifications for other weak far-UV emission lines are marked. The associated O VI absorption lines are indicated. All other absorption lines are foreground Galactic or intergalactic features. Bottom: the section of the *FUSE* spectrum surrounding the peak of the broad O VI emission line is shown. The spectrum is binned to a resolution of 0.12 Å (20 pixels) to show the continuum and emission lines more clearly. The three associated O VI absorption systems are marked, as well as the corresponding locations expected for Lyβ absorption. The Fe II feature is foreground Galactic absorption.

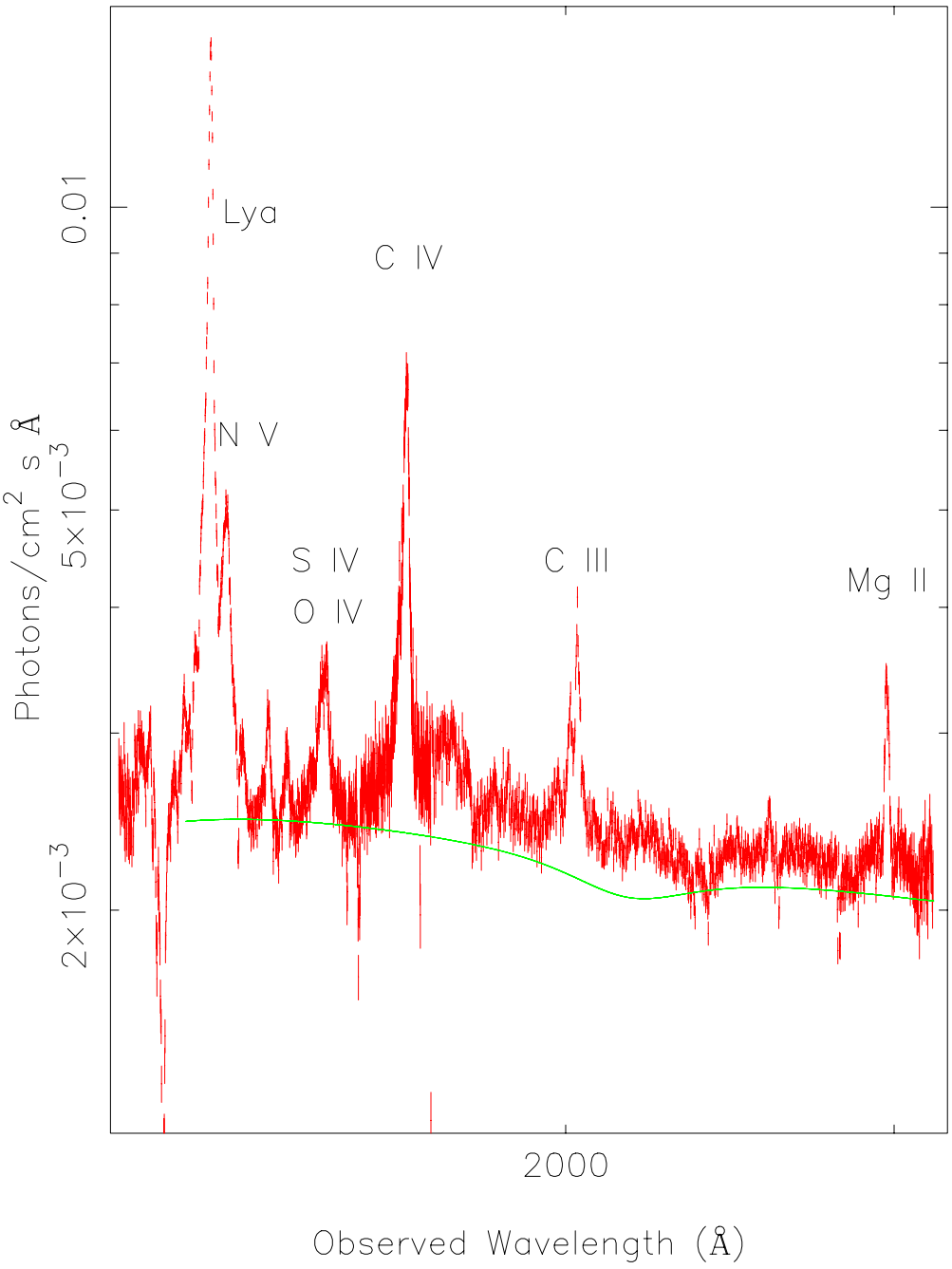

Fig. 5.— The *HST* STIS (1150–3150 Å) data, the solid line shows a power-law of energy index $\alpha = 0.66$ convolved with extinction by E(B-V)=0.0296, (i.e. neither the data or model has absorption correction). The strong lines are labelled, lines are tabulated in detail in Table 3.

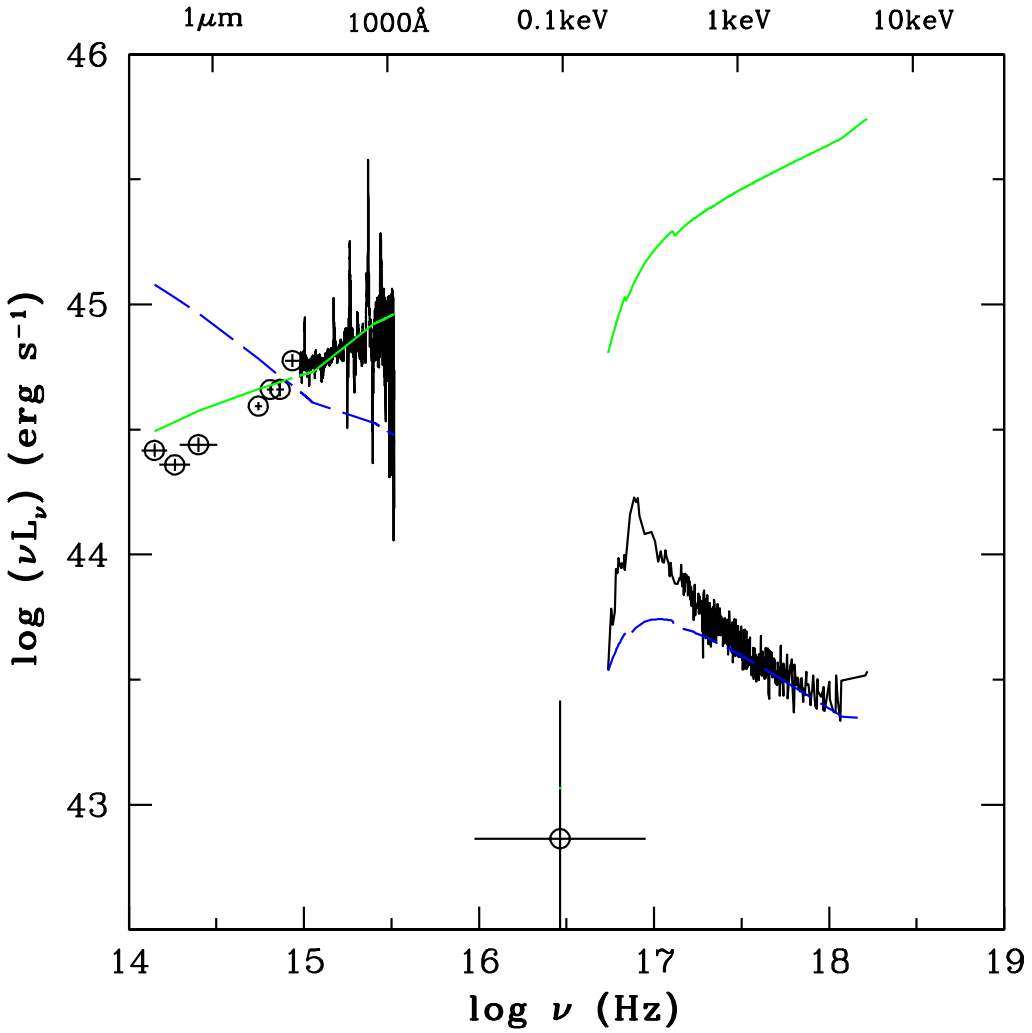

Fig. 6.— The multi-waveband data for Ton S180. In this plot, the data have not been corrected for absorption. The blue dashed line shows the (absorbed) power-law $\alpha = 1.44$ from the 2-10 keV regime, extrapolated to lower energies. The green solid line shows the power-law $\alpha = 0.66$ (convolved with line-of-sight absorption) from the fit to the STIS and *FUSE* data, extrapolated to higher energies. The open point between log ν =16–17 Hz represents the *EUVE* data, the circles represent the ground-based data.

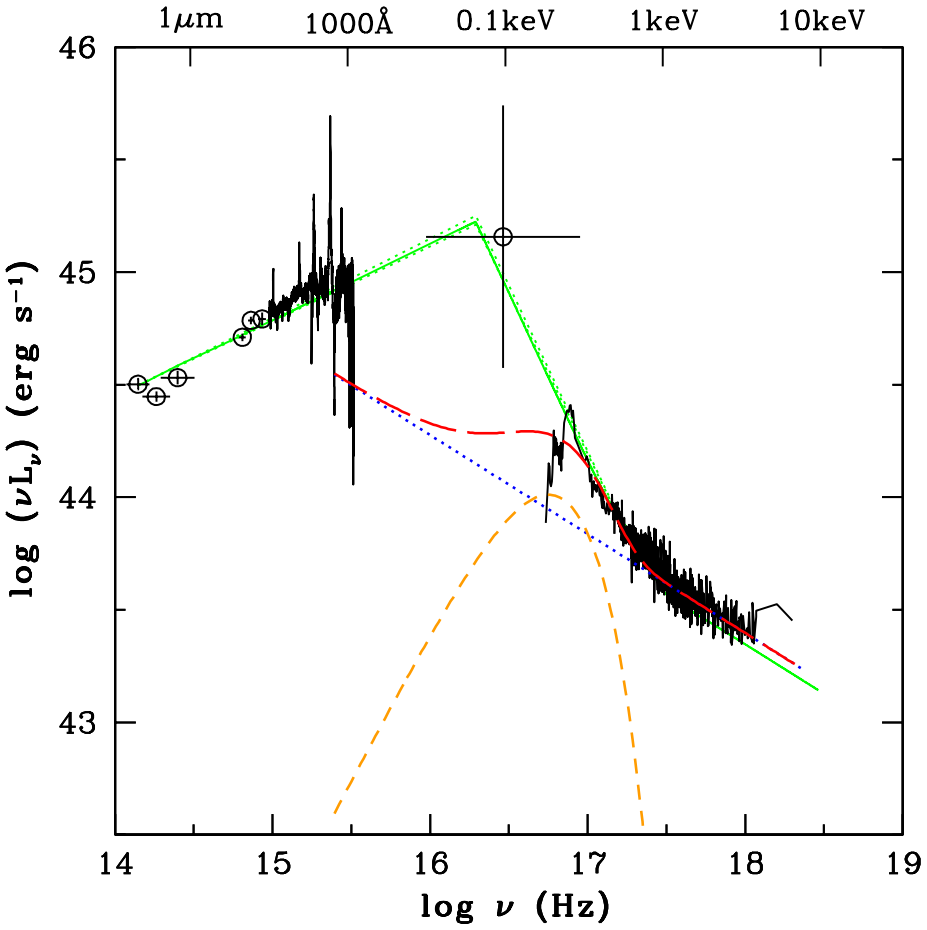

Fig. 7.— The Spectral Energy Distribution of Ton S180. The data presented here are shown as a solid black line. The data have been corrected for Galactic line-of-sight extinction. The circles represent the ground-based data. The simple model parameterization of the SED is shown as a solid green line. The dotted green line straddling this shows the uncertainty in the SED due to uncertainty in the galactic line-of-sight absorption. The dashed orange line is the blackbody and the dotted blue line the power-law model components of the SED, the red dashed line is their sum.

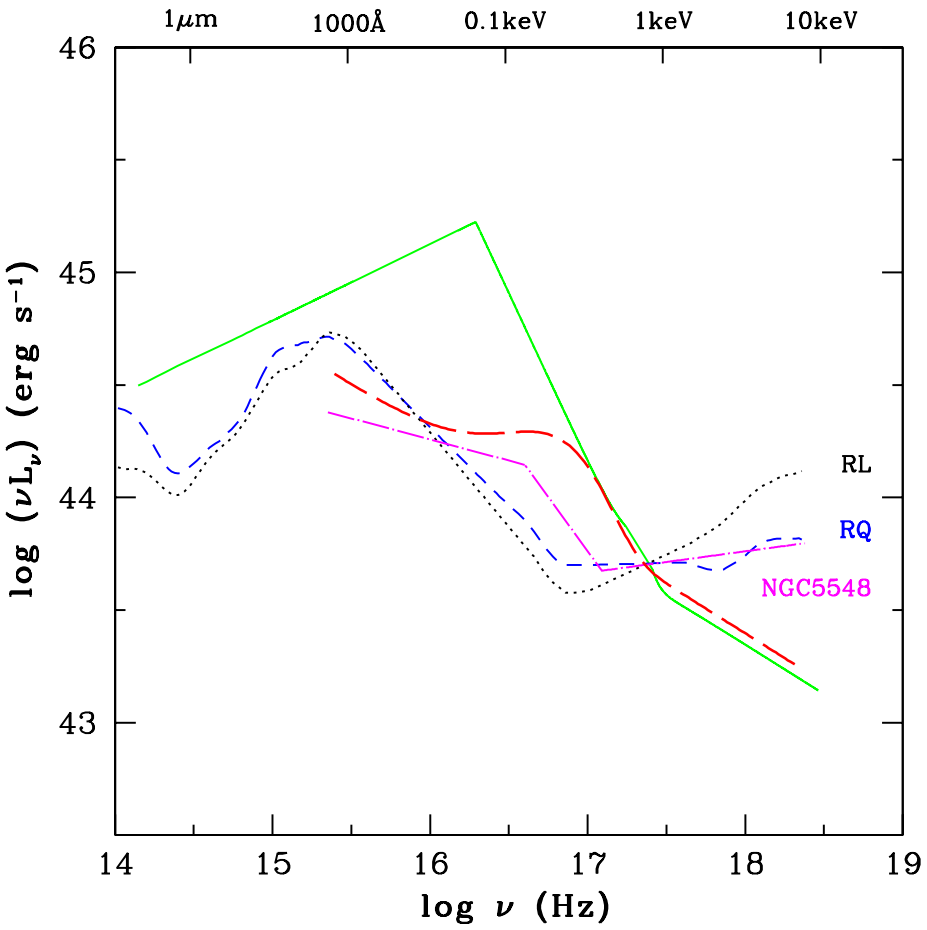

Fig. 8.— The Spectral Energy Distribution of Ton S180, represented by the solid green line from the simple parameterization. The dashed red line shows the sum of the blackbody and power-law model components (as in Figure 7). For comparison, the mean SED for radio-loud and radio-quiet quasars are also shown as dotted black and dashed blue lines, respectively (Elvis et al. 1994). The SED of NGC 5548 (a Sy1.5) is shown as a magenta dash-dot line (Kraemer et al. 1998).